Phonon densities of states and vibrational entropies of ordered and disordered Ni_3Al

B. Fultz, L. Anthony,* and L. J. Nagel
California Institute of Technology, MS 138-78, Pasadena, California 91125

R. M. Nicklow and S. Spooner
Oak Ridge National Laboratory, P.O. Box 2008, Oak Ridge, Tennessee 37831
(Received 13 January 1995)

We performed inelastic neutron-scattering measurements on powdered Ni_3Al. The alloy was prepared in two states of chemical order: (1) with equilibrium $L1_2$ order, and (2) with disorder (the material was a fcc solid solution prepared by high-energy ball milling). Procedures to convert the energy loss spectra into approximate phonon density of states (DOS) curves for Ni_3Al in the two states of chemical order were guided by Born–von Kármán analyses with force constants obtained from previous single-crystal experiments on $L1_2$-ordered Ni_3Al and fcc Ni metal. The main difference in the phonon DOS of the ordered and disordered alloys occurs near 39 meV, the energy of a peak arising from optical modes in the ordered alloy. These high-frequency optical modes involve primarily the vibrations of the aluminum-rich sublattice. The disordered alloy, which does not have such a sublattice, shows much less intensity at this energy. This difference in the phonon DOS around 39 meV is the main contributor to the difference in vibrational entropy of disordered and ordered Ni_3Al, which we estimate to be $S_{vib}^{dis}-S_{vib}^{ord}=(+0.2\pm0.1)k_B$/atom at high temperatures.

I. INTRODUCTION

There has been recent interest in the importance of vibrational entropy S_{vib} on the thermodynamic stabilities of alloy phases.[1–5] The possibility that vibrational entropy could affect chemical order-disorder transitions was recognized quite some time ago.[6–11] Since the work of Ising[12] and Bragg and Williams,[13] however, the thermodynamic stabilities of ordered alloys have almost always been explained with a free energy that includes only the configurational entropy S_{config} associated with the combinatorics of arranging the atoms on the crystal lattice sites.[14–16] It is possible to associate changes in S_{config} with the movements of atoms between lattice sites, and changes in S_{vib} with differences in the vibrations of the atoms about their lattice sites.

More recently, the inclusion of vibrational entropy in *ab initio* calculations with the Debye-Grüneisen approximation has suggested that vibrational entropy differences may shift the temperatures of phase boundaries by as much as 20%.[17,18] Scaling the phonon vibrational frequencies with the elastic constants may be an unreliable practice, however. For Cu_3Au, for example, the elastic constants are largely unaffected by the state of order in the alloy,[19,20] but the phonon density of states (DOS) undergoes large changes at high energies.[21,22] Large changes in the short-wavelength phonons are generally expected when chemical order develops; the formation of a superlattice decreases the size of the Brillouin zone and optical modes appear in the vibrational spectrum.

In addition to results on ordered and disordered Cu_3Au,[21] inelastic-neutron-scattering experiments have provided phonon dispersion curves for Fe_3Al in both its ordered and disordered states.[23–25] Analysis of the changes in the phonon DOS of Fe_3Al showed that the high-energy optical modes of the ordered alloy were able to account for the difference in vibrational entropy between disordered and $D0_3$-ordered Fe_3Al.[5] The present paper tests this idea for another transition metal aluminide, Ni_3Al. Previous calorimetric measurements showed the difference in vibrational entropy of ordered and disordered Ni_3Al to be about $0.3k_B$/atom,[2] which is a large fraction of the difference in configurational entropy ($\leq 0.57k_B$/atom). We hypothesize that the formation of a sublattice of stiffly bonded, light aluminum atoms in the $L1_2$ structure of Ni_3Al causes the ordered state to have a lower vibrational entropy than the disordered state. Although a neutron-inelastic-scattering experiment has been performed on a single crystal of Ni_3Al with $L1_2$ order,[26] it is unfortunately impossible to prepare single-crystal specimens of disordered fcc Ni_3Al. Measurements of neutron inelastic coherent scattering from single crystals therefore cannot be used to identify the differences in the types of phonons in ordered and disordered Ni_3Al. The present experiment was designed to provide some of this information by inelastic incoherent and coherent scattering from polycrystalline powders.

II. EXPERIMENT

Powders of Ni_3Al were made by mechanical alloying.[27,28] Measured amounts of elemental nickel and aluminum powders were milled in a Spex 8000 mixer/mill with hardened steel vials and stainless steel balls and a ball-to-powder weight ratio of 2:1. With hexane added to the vial, nearly complete alloying occurred in 3–4 h, and several batches of Ni_3Al powder were prepared by milling for 8 h at room temperature. X-ray diffractometry was performed with an Inel CPS-120 diffractometer using Co $K\alpha$ radiation. The total absence

0163-1829/95/52(5)/3315(7)/$06.00

of the (100) and (110) superlattice diffractions in the as-milled material, also seen in its neutron-diffraction pattern, showed that the as-milled powder was essentially without $L1_2$ long-range order (LRO). Figure 1 presents an x-ray-diffraction pattern from the as-milled powder, and a pattern from the same powder after annealing at 450°C for 10 h, which was the annealing treatment we used to produce $L1_2$ LRO in our samples.[29–31]

Samples of the as-milled and the annealed powders, each about 50 g, were placed in thin-walled aluminum cans and mounted on the goniometer of the HB3 triple-axis spectrometer at the High Flux Isotope Reactor at the Oak Ridge National Laboratory. The spectrometer was operated in constant-Q mode with the fixed final energy E_f being 14.8 meV. The energy loss spectra were made by scanning the incident energy from 14.8 to 64.8 meV. The neutron flux from the monochromator was monitored with a fission detector, which was used to control the counting time for each data point. The incident beam on the pyrolytic graphite monochromator crystal was collimated with 40′ slits, and 40′ slits were also used between the monochromator and the sample. Pyrolytic graphite filters placed after the sample were used to remove the $\lambda/2$ contamination. The filtered beam passed through 80′ slits before the pyrolytic graphite analyzer crystal. Following the analyzer, 2° slits were used before the ^{3}He detector. With this arrangement, the energy resolution varied from about 2 meV at low energy transfer to 5 meV at 40 meV energy transfer. (In addition to these instrument parameters, several runs were performed with other instrument resolutions. Agreement between these different data sets was good.) Four values of Q were chosen for each specimen, ranging from 3.23 to 4.23 Å^{-1}.

III. RESULTS

Energy loss spectra from the ordered and disordered Ni_3Al are presented in Fig. 2. Individual runs were highly reproducible, as shown by the two independent (but nearly coincident) data sets from the ordered alloy with $Q=4.23$ Å^{-1}. Effects from the broad transverse band of phonon states are seen in all data sets from 12 to 28 meV, and some structure is visible in this region. The energy loss spectrum from the material with $L1_2$ order also shows a peak around 39 meV. This peak was found in the calculated phonon DOS obtained from the results of single-crystal experiments by Stassis *et al.*[26] Examination of the eigenvectors of the dynamical matrix (see Sec. IV B) showed that it is attributable to optical modes dominated by the motions of the aluminum-rich sublattice. As discussed below, the intensity of this peak is suppressed in the present experiments, owing to the smaller scattering cross section of aluminum than that of nickel, and the relatively small vibrational amplitudes of the nickel atoms in these optical modes. No distinct peak at 39 meV is seen in the data from the disordered Ni_3Al, although some residual intensity is found around this energy. The peak at 33 meV for the disordered alloy is at approximately the same energy as the peak of the longitudinal modes for fcc nickel metal. Another distinct feature of the spectra from the disordered alloy is the stronger scattering intensity at energy losses below 10 meV or so.

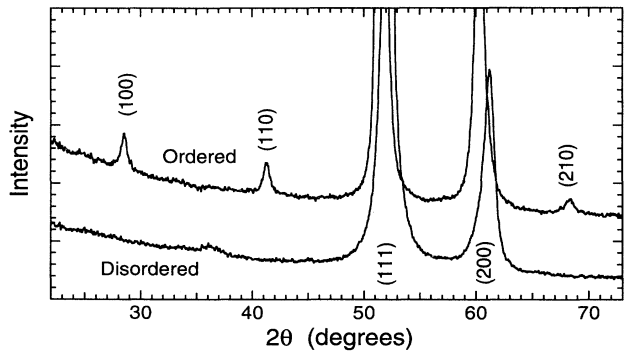

FIG. 1. X-ray powder-diffraction patterns of the ordered and disordered Ni_3Al powders, in the region of the (100) and (110) superlattice diffractions.

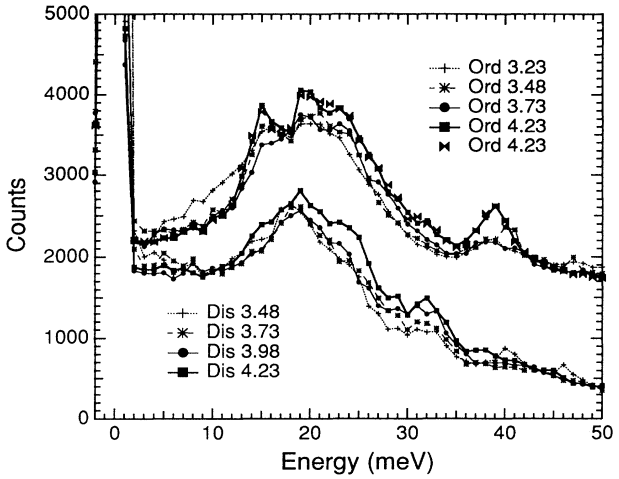

FIG. 2. Raw neutron energy loss spectra for the ordered and disordered Ni_3Al powders, obtained at four values of Q. Data for the ordered alloy are offset vertically by 1500 counts.

IV. ANALYSIS OF PHONON DOS

A. Calculated phonon DOS

The analysis of the scattering data from the ordered powder was helped considerably by the availability of previous phonon dispersion measurements on single crystals of $L1_2$ Ni_3Al.[26] Although the force constants were published, we were unable to use them satisfactorily in a Born–von Kármán model. Independent fits[32] to the experimental phonon dispersion curves of Ref. 26 provided the following set of force constants:

$$\left\{\phi_{xx}\begin{bmatrix}1\\12\end{bmatrix}=16.984,\ \phi_{xx}\begin{bmatrix}1\\22\end{bmatrix}=18.882,\right.$$

$$\phi_{zz}\begin{bmatrix}1\\12\end{bmatrix}=-1.128,\ \phi_{zz}\begin{bmatrix}1\\22\end{bmatrix}=-0.376,$$

$$\phi_{xy}\begin{bmatrix}1\\12\end{bmatrix}=18.112,\ \phi_{xy}\begin{bmatrix}1\\22\end{bmatrix}=19.258,$$

$$\phi_{xx}\begin{bmatrix}2\\11\end{bmatrix}=1.48,\ \phi_{xx}\begin{bmatrix}2\\22\end{bmatrix}=-1.38,$$

$$\left.\phi_{yy}\begin{bmatrix}2\\11\end{bmatrix}=1.864,\ \phi_{yy}\begin{bmatrix}2\\22\end{bmatrix}=0.645\right\}\ (\mathrm{N/m})\ .$$

The force constants are of the form

$$\phi_{\alpha\beta}\begin{bmatrix}\iota\\ \kappa\kappa'\end{bmatrix},$$

where α and β are the indices of the force constant tensor, ι specifies the nearest-neighbor distance, and κ and κ' indicate the sublattice pair, with Al atoms occupying sublattice 1 and Ni atoms occupying sublattice 2. Using these force constants, the dynamical matrix $\mathbf{D}(\mathbf{k})$ was diagonalized for approximately 10^6 values of $\mathbf{k}$ distributed uniformly over the first Brillouin zone. Histogram binning of the resulting eigenfrequencies provided the phonon DOS, presented at the top of Fig. 3(a). The dynamical structure factors were calculated simultaneously.

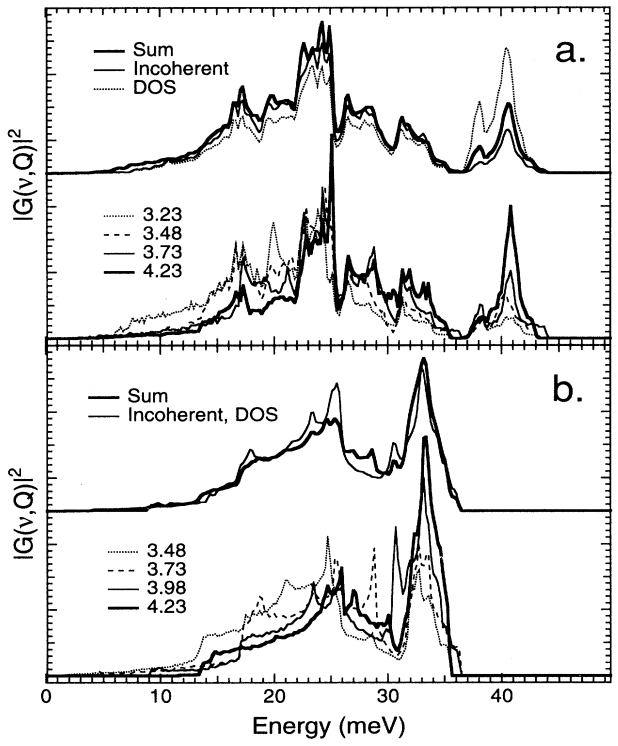

FIG. 3. (a) Calculations for $L1_2$ Ni_3Al. Top: phonon DOS, incoherent scattering spectrum, and average of all data at the bottom of (a). Bottom: total inelastic scattering (incoherent plus angle-averaged coherent) for $L1_2$ Ni_3Al at various values of Q. (b) Calculations for fcc Ni. Top: phonon DOS, incoherent scattering spectrum, and average of all data at the bottom of (b). Bottom: total inelastic scattering (incoherent plus angle-averaged coherent) for fcc Ni at various values of Q.

Truncating the force constants at second-neighbor distances provides a reasonable but imperfect fit to the phonon dispersion curves, and there are some differences between our phonon DOS and that of Stassis *et al.*[26] The present force constants are nevertheless adequate for identifying trends in the scattering intensity versus Q.

B. Calculated dynamical structure factors

Also shown at the top of Fig. 3(a) is the dynamical structure factor intensity for incoherent scattering of phonons of frequency ν, $|G_{\mathrm{inc}}(\nu,\mathbf{Q})|^2$, obtained from the Born–von Kármán model as the following sum[33] [with a factor involving the projection of the momentum transfer $\mathbf{Q}$ on the polarization vector $\sigma_d^\gamma(\mathbf{q})$ for the atom of mass M_d at the position d of the phonon in the branch γ with wave vector $\mathbf{q}$]:

$$|G_{\mathrm{inc}}(\nu,\mathbf{Q})|^2=\sum_d\frac{\sigma_{\mathrm{inc},d}}{M_d}\sum_\gamma\sum_{\mathbf{q}}|\mathbf{Q}\cdot\sigma_d^\gamma(\mathbf{q})|^2\times\delta(\nu-\nu_\gamma(\mathbf{q}))\ . \quad (1)$$

For each atom, branch, and $\mathbf{q}$, the crystallographic average of Eq. (1) over the various directions of $\mathbf{Q}$ is $\sigma_{\mathrm{inc},d}Q^2|\sigma_d^\gamma(\mathbf{q})|^2/3M_d$. This contribution to $|G_{\mathrm{inc}}(\nu,\mathbf{Q})|^2$ was binned during the phonon DOS calculation, as was the contribution to the partial phonon DOS, $|\sigma_d^\gamma(\mathbf{q})|^2$. The peak at 39 meV is suppressed considerably in the dynamical structure factor intensity for incoherent scattering. The partial phonon DOS for the aluminum and nickel atoms [essentially Eq. (1) with the $d=1$ (Al) or $d=2$ (Ni) terms only] showed that at the energies around 39 meV the aluminum atoms have much larger vibrational amplitudes than do nickel atoms. However, the incoherent scattering from aluminum is negligible ($\sigma_{\mathrm{inc}}<0.01$ b) compared to that of nickel ($\sigma_{\mathrm{inc}}=5.0$ b),[33] so incoherent scattering around 39 meV is rather weak.

The dynamical structure factor intensity for coherent scattering, $|G_{\mathrm{coh}}(\nu,\mathbf{Q})|^2$, was calculated as[33]

$$|G_{\mathrm{coh}}(\nu,\mathbf{Q})|^2=\sum_d\frac{1}{M_d}\sum_\gamma\sum_\tau\sum_{\mathbf{q}}|b_d\mathbf{Q}\cdot\sigma_d^\gamma(\mathbf{q})e^{i\mathbf{Q}\cdot d}|^2\times\delta(\nu-\nu_\gamma(\mathbf{q}))\times\delta(\mathbf{Q}-\mathbf{q}-\tau)\ , \quad (2)$$

where τ is a reciprocal lattice vector and b_d is the coherent scattering length. The crystallographic average of the inelastic coherent scattering required an evaluation of the dynamical structure factor intensity at explicit values of $\mathbf{Q}$ with respect to the crystallographic axes. For a given value of Q, the directions of $\mathbf{Q}$ were chosen with an isotropic probability distribution using a Monte Carlo sampling procedure.

Results for the total scattering, inelastic coherent plus inelastic incoherent, are presented at the bottom of Fig. 3(a). Differences in the shape of the curves with different Q are caused by the inelastic coherent scattering, whose variation with Q depends in a complicated way on the phonon DOS and relationships between $\mathbf{Q}$ and the Bril-

louin zone boundary.[34] Our calculations reproduce some of the detailed Q dependence of the experimental data on ordered Ni_3Al. For example, the strong scattering observed for $Q=3.23$ Å^{-1} around 10 meV is reproduced well in the calculation. The general trend for the scattering at higher energies to increase with Q is also reproduced well.

The top of Fig. 3(a) also shows the average of the four calculated curves at the bottom of Fig. 3(a), each normalized to unity. It differs from the phonon DOS curve primarily in its overemphasis of the low-energy part of the spectrum and underemphasis of the higher-energy part of the spectrum. (This average is similar, but not identical, to the dynamical structure factor intensity for incoherent scattering.) Dividing the phonon DOS by this average provided a "dynamical structure factor correction function" with a shape much like a step function, having an amplitude of 0.69 for energies below 35 meV and an amplitude of 1.94 for energies above 35 meV. For correction of the summed experimental data, the step in the dynamical structure factor correction function was smoothed by a Gaussian function with a full width at half maximum of 4 meV, the expected experimental resolution.

The analysis for the disordered alloy is more problematic, since force constants are not available from previous work. We began by assuming that the phonon DOS of the disordered Ni_3Al was the same as that of fcc Ni metal.[35] Starting with this phonon DOS of a typical fcc metal, we devised two methods for the analysis of the energy loss spectra from disordered Ni_3Al. The top of Fig. 3(b) shows the phonon DOS of fcc nickel. (For a monatomic crystal, as assumed in the virtual crystal approximation, the phonon DOS has the same shape as the dynamical structure factor intensity for incoherent scattering.) Also shown in Fig. 3(b) are the total incoherent plus coherent structure factor intensities from fcc nickel at the different values of Q used in the experiment. The average of these total inelastic scattering intensities is presented at the top of Fig. 3(b). We obtained a dynamical structure factor correction function for converting the inelastic scattering intensity into a phonon DOS, but it was not used for the analysis presented below. This correction function was roughly constant in energy, so in one approach for data analysis we assumed the correction factor to be unity. It certainly can be argued that the virtual crystal approximation is unreliable; the vibrational spectrum of the disordered crystal must be different from that of a monatomic fcc crystal. The experimental data do show that there is some intensity in the regions of the optical modes at 39 meV, presumably due to vibrations of aluminum atoms in local regions of partial order (light Al atoms vibrating in a cage of Ni atoms[5,36]). So as a second method for analysis of the data from the disordered alloy, we converted the summed inelastic scattering intensity into an approximate phonon DOS by using the same dynamical structure factor correction function as was used for the ordered alloy (the step function with a jump at 35 meV). We do not know which method for data analysis is more appropriate, so in what follows we present both.

C. Temperature

Another step in obtaining the phonon DOS involved the correction for the phonon populations in the different modes. We calculated the inelastic incoherent scattering using the conventional multiphonon expansion.[37–39] The calculation was performed for room temperature with the phonon DOS curves presented at the tops of Figs. 3(a) and 3(b). The results showed that, at the relatively low values of Q and temperature of the present experiments, the inelastic scattering is strongly dominated by one-phonon processes. Multiphonon corrections would have made little difference to the resultant phonon DOS, so these corrections were not performed. Also, our normalization of individual data sets, discussed below, eliminated the need to correct for the Debye-Waller factor suppression of the scattered intensity for larger values of Q. We do neglect differences in how the Debye-Waller factors for nickel and aluminum atoms change with Q, but these differences are not important because they are not large, and the scattering is dominated by the nickel atoms.

D. Data analysis procedure

The features of the calculated scattering (Secs. IV B and IV C) led us to the following procedure for obtaining an approximate phonon DOS from the experimental data of Fig. 2. Our data analysis procedure has some similarities to methods used previously.[38–42] The individual data sets for both the ordered and disordered alloys were corrected by subtracting the same constant background from all data sets, which is a good approximation for data from the HB3 spectrometer. Each background-corrected spectrum was divided by the one-phonon correction factor, $[n(\nu)-1]/\nu$,[33]

$$\frac{n(\nu)-1}{\nu}=\frac{1}{\nu[1-\exp(-h\nu/kT)]}\ . \tag{3}$$

Next, the individual spectra for the four values of Q for the disordered and ordered alloys were individually normalized to unity and then summed. Finally, the summed data for the ordered alloy were multiplied by the dynamical structure factor correction function, and this result was normalized to unity. The resulting approximate phonon DOS for the ordered alloy is presented in Fig. 4. As mentioned in Sec. IV B, we are uncertain if the disordered alloy can be treated as a virtual fcc crystal, or if we should use a correction factor as in the ordered alloy to weigh more heavily the data at higher energies. We expect that these two assumptions provide reasonable upper and lower bounds on the actual phonon DOS, so both results are presented in Fig. 4.

V. DISCUSSION

A. Phonon DOS

The phonon DOS of the ordered alloy presented in Fig. 4 is in reasonably good agreement with the phonon DOS reported by Stassis *et al.*[26] For comparison with the phonon DOS at the top of Fig. 3(a), we convolved the calculated data with a Gaussian function of width 4 meV.

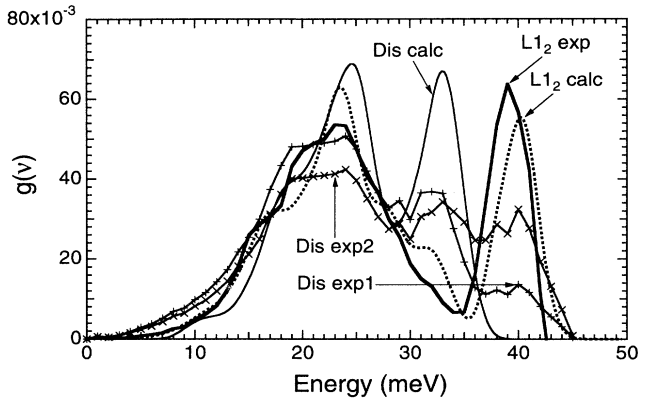

FIG. 4. Phonon DOS obtained by processing the experimental data of Fig. 2. The curve "$L1_2$ exp" was obtained from the data from the annealed powder with the $L1_2$ structure. The two curves "Dis exp1" and "Dis exp2" were obtained from the data from the as-milled powder, with two assumptions about the weighting of the observed intensity at high energies (see text, Sec. IV). The phonon DOS's at the tops of Figs. 3(a) and 3(b) were convolved with a Gaussian instrument function to provide the curves "$L1_2$ calc" and "Dis calc."

The overall agreement between the two curves ("$L1_2$ exp" and "$L1_2$ calc") is generally satisfactory. The peak at 39 meV in the calculated curve is a bit too large, however, having an integrated area of about 0.28, rather than the expected value of $\frac{1}{4}$. Discrepancies in the matching of the calculated and experimental $g(\nu)$ curves of the ordered alloy originate in part with our method of analysis, but also with the simplicity of the force constants (up to second-nearest neighbor only) used in the Born–von Kármán model.

For the disordered alloy, the experimental $g(\nu)$ curves show an enhanced intensity at energies around 10 meV. Some of this intensity could arise from the lifetime broadening of the phonon energies in the disordered alloy. It could also originate from the internal vibrations of the nanocrystallites produced by ball milling, hydrogen contamination of the specimen, or both. We do not expect these latter two problems to affect the phonon DOS of the disordered alloy at higher energies, however.

It is not surprising that there are significant differences in the experimental curves of the disordered Ni_3Al and the calculated phonon DOS curves of nickel, a monatomic fcc metal. The first difference is independent of our two methods of data analysis. In comparison to the calculated curve, the experimental $g(\nu)$ curves show a significantly weaker peak from longitudinal-mode phonons at 33 meV. Some of this loss of intensity could be associated with the lifetime broadening of the energy spectrum from the disordered alloy, but we believe the change in intensity is larger than expected for this mechanism. Another difference between the experimental and calculated phonon DOS of the disordered alloy is found around 39 meV. Because we do not know the different atom vibrations involved in this scattering, we cannot predict reliably the intensity around 39 meV. However, both our methods of data analysis provide some intensity in this energy range. This intensity is certainly suppressed considerably from its intensity in the ordered alloy, but it is nonnegligible. Both methods of processing the data from the disordered alloy suggest the presence of a bimodal high-energy structure with peaks around 33 and 39 meV. It is tempting to associate these peaks with the motions of nickel and aluminum atoms, respectively, but such a resolution cannot be justified rigorously.

B. Vibrational entropy

At high temperatures, the difference in vibrational entropy of the disordered and ordered Ni_3Al, $\Delta S_{\rm vib} \equiv S_{\rm vib}^{\rm dis} - S_{\rm vib}^{\rm ord}$, depends in a straightforward way on the difference in the phonon DOS of the two phases, $g^{\rm dis}(\nu) - g^{\rm ord}(\nu)$:

$$\Delta S_{\rm vib} = -3k_B \int_0^\infty [g^{\rm dis}(\nu) - g^{\rm ord}(\nu)] \ln(\nu) d\nu \ , \qquad (4)$$

where the difference avoids problems with the dimensions of the argument of the logarithm. When the phonon DOS of the disordered alloy was obtained from the virtual crystal approximation without any dynamical structure factor correction, Eq. (4) gave $\Delta S_{\rm vib} = 0.30 k_B$/atom. With the phonon DOS determined with the dynamical structure factor correction factor of the ordered alloy (i.e., with the assumption that the vibrations with energies above 35 meV involve primarily motions of aluminum atoms), $\Delta S_{\rm vib} = 0.10 k_B$/atom. For comparison, a value of $\Delta S_{\rm vib}$ somewhat less than $0.3 k_B$/atom was obtained by cryogenic calorimetry and by extended electron energy loss fine-structure spectroscopy measurements on evaporated thin films of Ni_3Al.[2]

Some of the contribution to $\Delta S_{\rm vib}$ from Eq. (4) is associated with the intensity of the phonon DOS of the disordered alloy at energies below 10 meV, but examination of the integrand $g^{\rm dis}(\nu)\ln(\nu)$ showed that this was not the major effect. The difference between the vibrational entropies of the ordered and disordered alloys is caused primarily by differences in the energy spectrum at higher energies near 39 meV. Because the ordered alloy has a sublattice of aluminum atoms, the high-frequency vibrational modes involving primarily these light but stiffly bonded atoms suppress the vibrational entropy of the ordered alloy. The present experiment shows that the vibrational spectrum of the disordered alloy has some intensity at the energies of the optical modes in the ordered alloy, but much less than for the ordered alloy. This effect of the optical modes is much the same as was proposed for Fe_3Al.[5] The present measurements suggest, however, that for the purpose of understanding the magnitude of vibrational entropy, it may be problematical to analyze the phonon DOS with a virtual crystal approximation. The lack of vibrational modes at high energies in the previous calculation for disordered bcc Fe_3Al may have been why the calculated phonon DOS curves for ordered and disordered Fe_3Al provided a $\Delta S_{\rm vib}$ that was larger than was obtained from calorimetry.[5]

VI. CONCLUSION

We performed inelastic neutron-scattering experiments on Ni_3Al in two states of chemical order: with $L1_2$ LRO

and as a disordered fcc solid solution. For each sample, energy loss spectra were collected at four values of Q. A Born–von Kármán analysis was performed with force constants obtained from single-crystal experiments, and the results from this analysis suggested a procedure for extracting an approximate phonon DOS from the energy loss spectra of the ordered alloy. The resulting phonon DOS was in good agreement with the phonon DOS obtained previously for $L1_2$ Ni_3Al. The spectra from the disordered alloy were also analyzed with this method, and by another method that assumed that the participation of the nickel and aluminum atoms in the scattering was independent of phonon energy.

The most significant difference in the phonon DOS of the ordered and disordered alloys was the prominent peak at 39 meV in the ordered alloy, corresponding to optical modes involving vibrations primarily of the aluminum-rich sublattice. The intensity near 39 meV was much weaker in the disordered alloy, but not negligible. The corrected phonon DOS curves of the disordered and ordered alloys were used to calculate a difference in vibrational entropy which was $S_{\rm vib}^{\rm dis}-S_{\rm vib}^{\rm ord}=(+0.2\pm0.1)k_B$/atom, in reasonable agreement with previous measurements by calorimetry. The main contribution to this difference in vibrational entropy was the difference in the phonon spectrum around 39 meV, which is the energy of optical modes involving vibrational motions of primarily the aluminum-rich sublattice of the ordered alloy.

ACKNOWLEDGMENTS

We thank B. Hennion for fitting the phonon dispersion curves of Ni_3Al (Ref. 26) with a Born–von Kármán model, and supplying us with a set of force constants. L. Preister performed much of the powder preparation. The Oak Ridge National Laboratory is managed for the Department of Energy by Martin Marietta Energy Systems, Oak Ridge, TN under Contract No. DE-AC05-84OR214000. This work was supported by the U.S. Department of Energy under Contract No. DE-FG03-86ER45270.

*Present address: University of Toledo, Dept. of Physics and Astronomy, Toledo, OH 43606-3390.

[1]J. K. Okamoto, C. Ahn, and B. Fultz, in *Microbeam Analysis–1990,* edited by J. R. Michael and P. Ingram (University of California, San Francisco Press, San Francisco, 1990), pp. 56–58.

[2]L. Anthony, J. K. Okamoto, and B. Fultz, Phys. Rev. Lett. **70**, 1128 (1993).

[3]S. J. Clark and G. J. Ackland, Phys. Rev. B **48**, 10 899 (1993).

[4]G. D. Garbulsky and G. Ceder, Phys. Rev. B **49**, 6327 (1994).

[5]L. Anthony, L. J. Nagel, J. K. Okamoto, and B. Fultz, Phys. Rev. Lett. **73**, 3034 (1994).

[6]C. Booth and J. S. Rowlinson, Trans. Faraday Soc. **51**, 463 (1955).

[7]P. J. Wojtowciz and J. G. Kirkwood, J. Chem. Phys. **33**, 1299 (1960).

[8]G. Moraitis and F. Gautier, J. Phys. F **7**, 1421 (1977).

[9]H. Bakker, Philos. Mag. A **45**, 213 (1982).

[10]J. A. D. Matthew, R. E. Jones, and V. M. Dwyer, J. Phys. F **13**, 581 (1983).

[11]H. Bakker and C. Tuijn, J. Phys. C **19**, 5585 (1986).

[12]E. Ising, Z. Phys. **31**, 253 (1925).

[13]W. L. Bragg and E. J. Williams, Proc. R. Soc. London Ser. A **145**, 699 (1934); **151**, 540 (1935).

[14]D. de Fontaine, Solid State Phys. **34**, 73 (1979).

[15]See, for example, F. Ducastelle, *Order and Phase Stability in Alloys* (North-Holland, Amsterdam, 1991).

[16]K. Terakura, T. Oguchi, T. Mohri, and K. Watanabe, Phys. Rev. B **35**, 2169 (1987); A. A. Mbaye, L. G. Ferreira, and A. Zunger, Phys. Rev. Lett. **58**, 49 (1987); A. E. Carlsson and J. M. Sanchez, Solid State Commun. **65**, 527 (1988); M. Sluiter, D. de Fontaine, X. Q. Guo, R. Podloucky, and A. J. Freeman, Phys. Rev. B **42**, 10 460 (1990).

[17]J. M. Sanchez, J. P. Stark, and V. L. Moruzzi, Phys. Rev. B **44**, 5411 (1991).

[18]T. Mohri, S. Takizawa, and K. Terakura, J. Phys. Condens. Matter **5**, 1473 (1993).

[19]J. A. Rayne, Phys. Rev. **108**, 649 (1975).

[20]P. A. Flinn, G. M. McManus, and J. A. Rayne, J. Phys. Chem. Solids **15**, 189 (1960).

[21]Y. Noda, Y. Endoh, S. Katano, and M. Iizumi, Physica B&C **120**, 317 (1983).

[22]F. Cleri and V. Rosato, Philos. Mag. Lett. **67**, 369 (1993).

[23]C. Van Dijk, Phys. Lett. **34A**, 255 (1970).

[24]I. M. Robertson, Solid State Commun. **53**, 901 (1985).

[25]I. M. Robertson, J. Phys. Condens. Matter **3**, 8181 (1991).

[26]C. Stassis, F. X. Kayser, C.-K. Loong, and D. Arch, Phys. Rev. B **24**, 3048 (1981).

[27]J. S. C. Jang and C. C. Koch, J. Mater. Res. **5**, 498 (1990).

[28]T. Nasu, C. C. Koch, A. M. Edwards, and D. E. Sayers, J. Non-Cryst. Solids **150**, 491 (1992).

[29]S. R. Harris, D. H. Pearson, C. M. Garland, and B. Fultz, J. Mater. Res. **6**, 2019 (1991).

[30]A. R. Yavari, Acta Metall. Mater. **41**, 1391 (1993).

[31]M. D. Baró, S. Suriñach, J. Malagelada, M. T. Clavaguera-Mora, S. Gialanella, and R. W. Cahn, Acta Metall. Mater. **41**, 1065 (1993).

[32]B. Hennion (private communication).

[33]G. Kostorz and S. W. Lovesey, in *Neutron Scattering,* edited by G. Kostorz, Treatise on Materials Science and Technology Vol. 15 (Academic, New York, 1979), p. 1.

[34]F. W. de Wette and A. Rahman, Phys. Rev. **176**, 784 (1968).

[35]P. H. Dederichs, H. Schober, and D. J. Sellmyer, in *Phonon States, Electron States, and Fermi Surfaces,* edited by K.-H. Hellwege and J. L. Olsen, Landolt-Börnstein, New Series, Group III, Vol. 13a, Pt. 1.2 (Springer-Verlag, Berlin, 1981).

[36]This concept is illustrated by P. Dean, Rev. Mod. Phys. **44**, 127 (1972).

[37]V. F. Sears, Phys. Rev. A **7**, 340 (1973).

[38]J.-B. Suck and H. Rudin, in *Glassy Metals II,* edited by H. Beck and H.-J. Güntherodt (Springer-Verlag, Berlin, 1983), Chap. 7.

[39]D. D. Klug, E. Whalley, E. C. Svensson, J. H. Root, and V. F. Sears, Phys. Rev. B **44**, 841 (1991).

[40]J. Chevrier, J. B. Suck, M. Perroux, and J. J. Caponi, Phys. Rev. Lett. **61**, 554 (1988).
[41]C.-K. Loong, P. Vashishta, R. K. Kalia, W. Jin, M. H. Degani, D. G. Hinks, D. L. Price, J. D. Jorgensen, B. Dabrowski, A. W. Mitchell, D. R. Richards, and Y. Zheng, Phys. Rev. B **45**, 8052 (1992).
[42]J. Chevrier, J. B. Suck, J. C. Lasjanunias, M. Perroux, and J. J. Caponi, Phys. Rev. B **49**, 961 (1994).